

Continuous Borehole Strain and Pore Pressure in the Near Field of the 28 September 2004 **M** 6.0 Parkfield, California, Earthquake: Implications for Nucleation, Fault Response, Earthquake Prediction, and Tremor

by M. J. S. Johnston, R. D. Borchardt, A. T. Linde, and M. T. Gladwin

Abstract Near-field observations of high-precision borehole strain and pore pressure, show no indication of coherent accelerating strain or pore pressure during the weeks to seconds before the 28 September 2004 **M** 6.0 Parkfield earthquake. Minor changes in strain rate did occur at a few sites during the last 24 hr before the earthquake but these changes are neither significant nor have the form expected for strain during slip coalescence initiating fault failure. Seconds before the event, strain is stable at the 10^{-11} level. Final prerupture nucleation slip in the hypocentral region is constrained to have a moment less than 2×10^{12} N m (**M** 2.2) and a source size less than 30 m. Ground displacement data indicate similar constraints. Localized rupture nucleation and runaway precludes useful prediction of damaging earthquakes. Coseismic dynamic strains of about 10 microstrain peak-to-peak were superimposed on volumetric strain offsets of about 0.5 microstrain to the northwest of the epicenter and about 0.2 microstrain to the southeast of the epicenter, consistent with right lateral slip. Observed strain and Global Positioning System (GPS) offsets can be simply fit with 20 cm of slip between 4 and 10 km on a 20-km segment of the fault north of Gold Hill ($M_0 = 7 \times 10^{17}$ N m). Variable slip inversion models using GPS data and seismic data indicate similar moments. Observed postseismic strain is 60% to 300% of the coseismic strain, indicating incomplete release of accumulated strain. No measurable change in fault zone compliance preceding or following the earthquake is indicated by stable earth tidal response. No indications of strain change accompany nonvolcanic tremor events reported prior to and following the earthquake.

Introduction

High-resolution continuous strain records during and preceding moderate to large earthquakes in California and Japan have been reported previously (Johnston and Linde, 2002). The occurrence of the 28 September 2004, **M** 6.0 Parkfield earthquake in the middle of a borehole strainmeter array at Parkfield provides the best near-field strain data yet, before, during, and after an earthquake of this magnitude. These data, together with pore pressure, creep, and other data, reflect on issues of importance to source mechanics that include the mechanics of fault failure, nucleation of moderate to large earthquakes, the feasibility of earthquake prediction, the behavior of postseismic fault slip, the behavior of crustal materials within and near active faults, and seismic and aseismic failure. The data obtained generally support our previous observations, which follow:

1. Strain changes greater than 10^{-9} apparently are not observed during the period hours to seconds before the event where, based on both theoretical predictions (Rice

and Rudnicki, 1979) and laboratory experiments (Lockner, 1998), crack coalescence and growth should be expected with the associated strainfield most easily detectable. This places a strong constraint on nucleation source size and indicates nucleation runaway, or “cascade,” in the terminology of Ellsworth and Beroza (1995), as the likely failure mechanics. Consequently, it appears that prediction of the size, location, and occurrence time of moderate to large earthquakes will not be an easily achievable goal in earthquake science.

2. Coseismic strain changes observed for earthquakes are in general agreement with expectations from seismic and geodetic models. Separation of the earthquake rupture coseismic slip and immediate postseismic slip can be resolved with the strain data recorded for these earthquakes. This is an important issue for regions with fault creep like Parkfield since GPS displacement measurements averaged over 100 sec, 1 hr or 1 day to reduce the noise, may overestimate the moment because the measurements are

2

M. J. S. Johnston, R. D. Borchardt, A. T. Linde, and M. T. Gladwin

made over time periods that include coseismic slip and immediate postseismic slip.

3. Postseismic strain changes comparable to the strain release by the earthquake indicate continuing but decaying postseismic slip indicative of incomplete crustal stress release by this single M 6.0 earthquake.
4. Tidal response data indicate significant changes in near fault compliance as a precursor to, or consequence of, these earthquakes are not greater than about 5% if they occur at all.

The location of the mainshock epicenter and subsequent fault rupture in relation to the main trace and southwest trace of the San Andreas Fault at Parkfield is shown, together with the various instrument sites, in Figure 1. Preliminary seismic moment tensor inversion indicates a moment for the earthquake of about 10^{18} N m (M 6.0) that results predominantly from right-lateral faulting on the near-vertical main San Andreas Fault with some minor slip contributions on the southwest trace (Bakun *et al.*, 2005). The slip distribution along the rupture was mostly in a $N43^{\circ}W$ direction from the hypocenter at a depth of 7.9 km under Gold Hill and was initially localized between about 4 km and 8 km in depth where it reached a peak of just over 60 cm about 10 km north of the epicenter. The initial rupture length was about 20 km, and postseismic slip quickly broke through to the surface in the hours following the earthquake. Significant postseismic slip above and around the earthquake slip has continued in the months following the earthquake (Langbein *et al.*, 2006).

Inversions of strong-motion data (Chen *et al.*, 2004; Liu and Archuleta, 2004; Liu *et al.*, 2006) and geodetic data taken before and after the earthquake (Murray *et al.*, 2004, 2006; Langbein *et al.*, 2006) indicate similar moments although the slip profile for the geodetic inversion is deeper to the northwest than that derived from the seismic inversions. Joint inversion (Dreger *et al.*, 2004; Chen *et al.*, 2004) indicates a compromise slip distribution with a moment of 1.1×10^{18} N m.

In this article we show and discuss the implications of these high-resolution strain and pore pressure data recorded before, during, and following the M 6.0 Parkfield earthquake. The strain network we use was originally designed and installed some 20 years ago to capture this earthquake and, fortunately, operation has continued long enough for these data to be obtained. The original purpose for the network was to investigate the physics of fault failure and determine whether routine earthquake prediction might be possible. Because of the precision of these instruments was more than a thousand times greater than other geodetic techniques in the short term, this experiment provided our best chance at isolating some of these details.

Instrumentation

Our measurement system consists of five Sacks–Evertson dilatometers (Sacks *et al.*, 1971), two borehole tensor

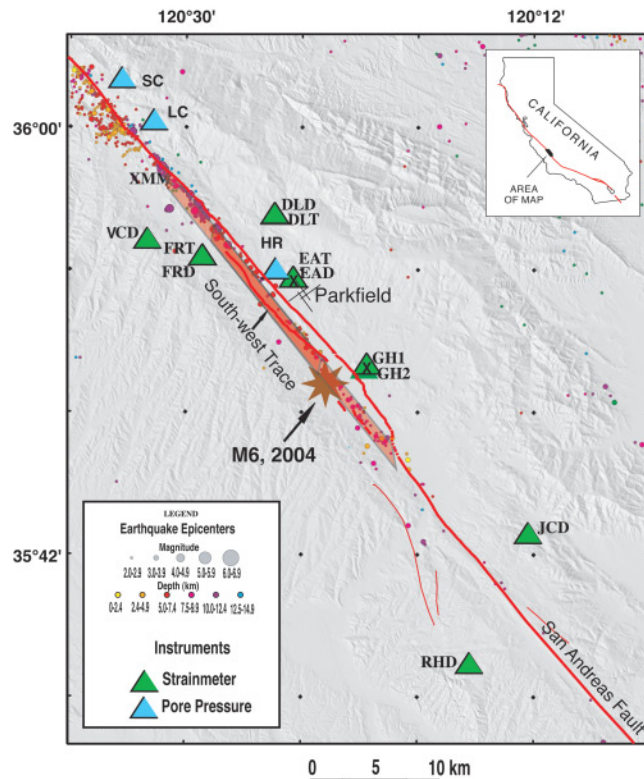


Figure 1. Locations of dilational strainmeters, tensor strainmeters, and pore pressure monitors in the Parkfield region relative to the epicenter and subsequent rupture of the 28 September 2004 M 6.0 Parkfield earthquake (star), its subsequent rupture plane (transparent box), and its subsequent aftershocks. Also shown with a black X are instruments (GH1, GH2, EAD, and EAT) that had ceased operation by the time of the earthquake. See Table 1 for detailed location information.

strainmeters (Gladwin, 1984), two pore pressure monitors (north of the rupture), and one water well (HR) (close to the fault near the peak slip of the earthquake). Locations of the instruments are shown in Figure 1. It is obvious that as a result of some correct site choices (and probably some luck), the earthquake epicenter is near the exact center of the array. The most important of these sites are FR and DL where both tensor (FRT, DLT) and dilational (FRD, DLD) strainmeters are installed on the west and east side of the fault near the region of peak slip from the earthquake. Dilatometers JCD and RHD are likewise installed on the east and west sides of the fault in the south. Unexplained long-term changes in the VCD instrument preclude using this instrument for long-term strain purposes. Most of the strain instrumentation was installed in 1986–87 in anticipation of the M 6.0 Parkfield earthquake. Several other dilatometers (GH1, GH2, EAD) and one tensor strainmeter (EAT) were installed earlier, but these instruments failed in the mid-1990s due to cable leakage. This is unfortunate since GH1 and GH2 were installed in 1982 almost right at the subsequent earthquake epicenter.

The strainmeters are installed in sandstone or granite units at depths that range from 118 m to 323 m, as shown in Figure 2a, using an expansive grout that has material properties similar to that of the host rock. Locations, depths, and rock types are listed in Table 1. The boreholes are filled to the surface with cement to reduce long-term strain changes due to hole relaxation effects and to avoid strains due to reequilibration of aquifer systems. At these depths, noise spectral levels have a red or $1/f^2$ character and have a range from -200 dB to -230 dB in the period band 1 sec to 0.01 seconds, from -100 dB to -150 dB from a month to hours and from -50 dB to -100 dB at periods from a year to a month. dB is referenced to 1 (strain)²/Hz. At periods of about 6 months, the noise level approaches that of GPS strain measurements (Johnston and Linde, 2002). Pore pressure monitors measure pressure in sealed aquifers at depths of 222 m (SC) and 195 m (LC). Installations are shown in schematic form in Figure 2b. The pore pressure instruments were installed in 2002.

All dilatometers, pore pressure, and the one water-well instrument transmit data every 10 min through a 16-bit digital telemetry system through the GOES satellite to the U.S. Geological Survey headquarters in Menlo Park, California (Silverman *et al.*, 1989). The tensor strainmeters sample every 18 min (DLT) and every 30 min (FLT) and also transmit their data by GOES satellite telemetry. The strain sensors, their installation, and the telemetry system are calibrated together against theoretical ocean-load corrected solid earth tides (Hart *et al.*, 1996; Linde *et al.*, 1992). This calibration is usually repeatable to better than 5%. The dilatometer data are also recorded in event trigger mode at different gains on 16-bit digital GEOS recorders at 200 samples per sec together

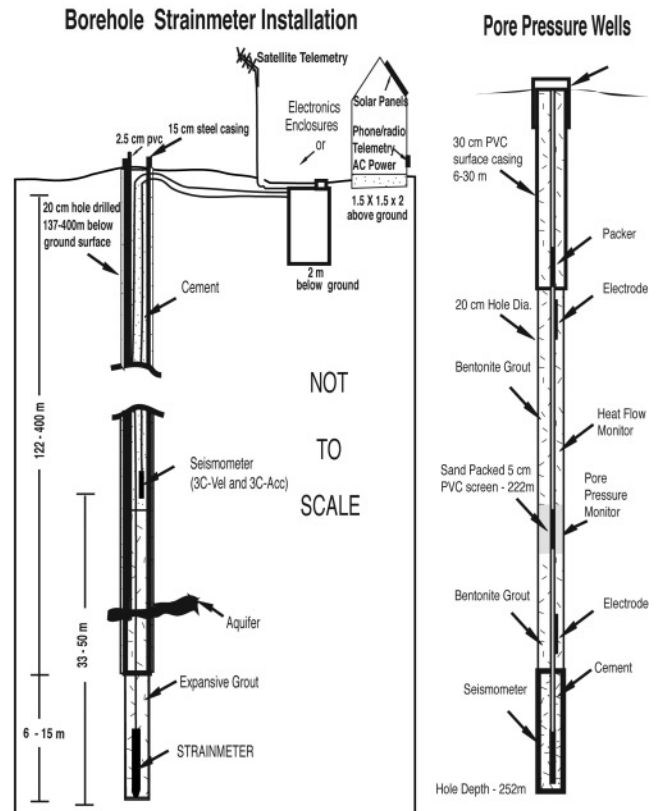


Figure 2. Schematics showing borehole strainmeter (left) and pore pressure installation (right) designs.

Table 1
Locations and Depths of the Various Borehole Strain and Pore Pressure Instrumentation

Site	Latitude	Longitude	Depth (m)	Altitude (m)	Install (dd/mm/yyyy)	Rock	Status
Dilatometers							
GH1	35.8314	-120.3461	117.6	510	6/27/1983	Granite	Dead
GH2	35.8372	-120.3445	177.7	507	7/01/1983	Granite	Dead
EAD	35.8946	-120.4220	267.2	595	10/24/1984	Sandstone	Dead
VCD	35.9219	-120.5355	204.1	940	11/24/86	Sandstone	OK
FRD	35.9108	-120.4883	323.36	674	12/6/86	Rhyolite	OK
DLD	35.9401	-120.4234	176.48	572	11/19/86	Sandstone	OK
RHD	35.6244	-120.2577	229.16	686	1/19/87	Sandstone	OK
JCD	35.7153	-120.2064	169.13	567	1/18/87	Sandstone	OK
Tensor Strain							
FRT	35.9107	-120.4859	237.3	674	12/7/86	Rhyolite	OK
DLT	35.9401	-120.4234	174.0	572	11/8/86	Sandstone	OK
EAT	35.8936	-120.4208	271.4	592	11/13/86	Sandstone	Dead
Pore Pressure							
LC	35.98006	-120.51423	195	637	7/24/01	Sandstone	OK
SC	36.0094	-120.53662	222	947	7/24/01	Granite	OK
Water Well							
WR	35.3145	-120.4250	134	782	2/16/1994	Sandstone	OK

with signals from colocated three-component seismic velocity and acceleration transducers (Borchardt *et al.*, 1985). Simultaneous seismic velocity, acceleration, and volumetric strain data have been recorded for the past 2 decades during events with $M > 3.0$ (Borchardt *et al.*, 2006). These recordings include up to 20 sec of preevent data.

Data

Figure 3a (upper plot) shows the 10-min (raw) dilational strain data with effects from changes in atmospheric pressure load and instrument resets removed during the period 18 September 2004 to 6 October 2004, before and after the Parkfield earthquake. In the convention used here, contraction is positive. Units are microstrain. Also shown Figure 3a (lower) are pore pressure and waterwell-level data. The sinusoidal-like signal in both data sets results from the earth tides. These are not removed at this stage to provide a continuous quality check on the data. These atmospheric pressure effects were removed by calculating the zero-frequency transfer function between pressure/strain and pressure/pore pressure and subtracting the pressure signal from each data set. Figure 3b (upper) shows the areal and tensor strains and tensor strain component data in microstrain for FRT, while Figure 3b (lower) shows the same data for DLT.

Main features of these data are as follows:

1. The absence of obvious variations in strain and pore pressure before the earthquake. This issue will be discussed in more detail later.
2. Compressional coseismic strain steps of about 0.3 microstrain on the west side and extensional strain offsets of about 0.6 microstrain east side of the fault in the north and opposite though smaller steps in the south as expected for failure of a right-lateral strike-slip fault.
3. Postseismic strain reaching as much as 200% of the coseismic occurred in the 24 hr following the earthquake, and over the subsequent six months has reached as much as 600% at some sites.

Because we record surface three-component acceleration and velocity onsite at 200 samples per sec (sps) together with borehole strain data at all sites, the details of the actual coseismic offset and short-term preseismic data were well recorded. The strain and the acceleration data are discussed in Borchardt *et al.* (2006) and the strain data are shown in Figure 4 for the various sites. In each summary, the upper plots show three days of satellite data, and lower plots show high sample rate strain data. In every case, the dynamic strains are at least 10 times larger than the static strains in the near field and more than 100 times larger in the intermediate to far-field reflecting the $1/r^3$ fall-off in the static strain with distance and $1/r^2$ falloff in dynamic strain. The VC instrument reset, not with the mainshock but after an aftershock, 4.5 min following the main event. We are able to reconstruct the offset using the triggered data from the

high-sample rate onsite recorder since these data during aftershocks track the background strain level. A 4.6 microstrain correction to the VC data indicated by the triggered data has been applied.

If all these strain data are high-pass filtered, the resulting straingram tracks the velocity record well during the arrival of the early dilational phases, as expected from theory (Borchardt *et al.*, 1989) and shown in practice (Borchardt *et al.*, 2006).

Coseismic Strain and Pore Pressure

Offsets generated by the Parkfield earthquake, listed in Tables 2 and 3, are shown in Figure 3a and 3b. The offsets from 10-min dilatometer data, and 18-min and 30-min tensor-strain data for the Parkfield earthquake are larger than the coseismic offsets recorded at high sample rate during the first 30 sec of the earthquake (Borchardt *et al.*, 2006) as a result of postseismic slip continuing to occur following the earthquake. As a consequence of the different sample times, the coseismic areal strain data from the two sites with both dilational and tensor strain are slightly different. For example, the coseismic areal strain at dilatometer site DLD taken 5 min after the earthquake is -0.56 microstrain, while the coseismic areal strain from the tensor site DLT taken 25 min after the earthquake is -0.85 microstrain. The slower sample rate data were initially combined with 100-sec coseismic GPS data to obtain a simple slip model shown in Figure 5 (upper). The fits to the strain data are not better than 10% of the observed offsets. Nevertheless, all of the slip appears to be to the north of the **M** 6.0 hypocenter between this and the 1966 hypocenter from 4- to 10-km depth and with a slip of 35 cm. The background from Fletcher and Spudich (1998) shows patches of fault slip that occurred with four **M** 4–5 earthquakes in 1992, 1993, and 1994 that triggered increased fault displacement in this region Langbein *et al.* (1999).

Variable slip models have been developed by Langbein *et al.* (2005, 2006), Murray and Langbein (2006), and Chen *et al.* (2004) based on inversion of GPS data alone. These models are shown in Figure 5 (middle, lower). Observed and calculated strains at each site are listed in Table 4. The best fit to the observed strains comes from the Langbein *et al.* (2006) model, but small changes in model geometry can produce significant changes in strain. It would appear that joint inversion of 20-sec strain data, comparable GPS data, and seismic data in these variable slip models will be necessary to produce a final best-fitting model without contamination from postseismic slip. As mentioned above, postseismic slip contamination is very apparent in the strain data for this earthquake. Coseismic strain offsets obtained from the 200 sps data on the same instrument are 40% less than the coseismic strains sampled at 5 min after the event (Borchardt *et al.*, 2006). At higher sample rates (1 Hz), the GPS resolution is poor (≈ 2.5 cm *P-P*) and, if the GPS data are averaged over longer periods to reduce noise (even 100 sec), postseismic deformation is continuing and this will be

Continuous Borehole Strain and Pore Pressure in the Near Field of the 28 September 2004 *M* 6.0 Parkfield Earthquake

5

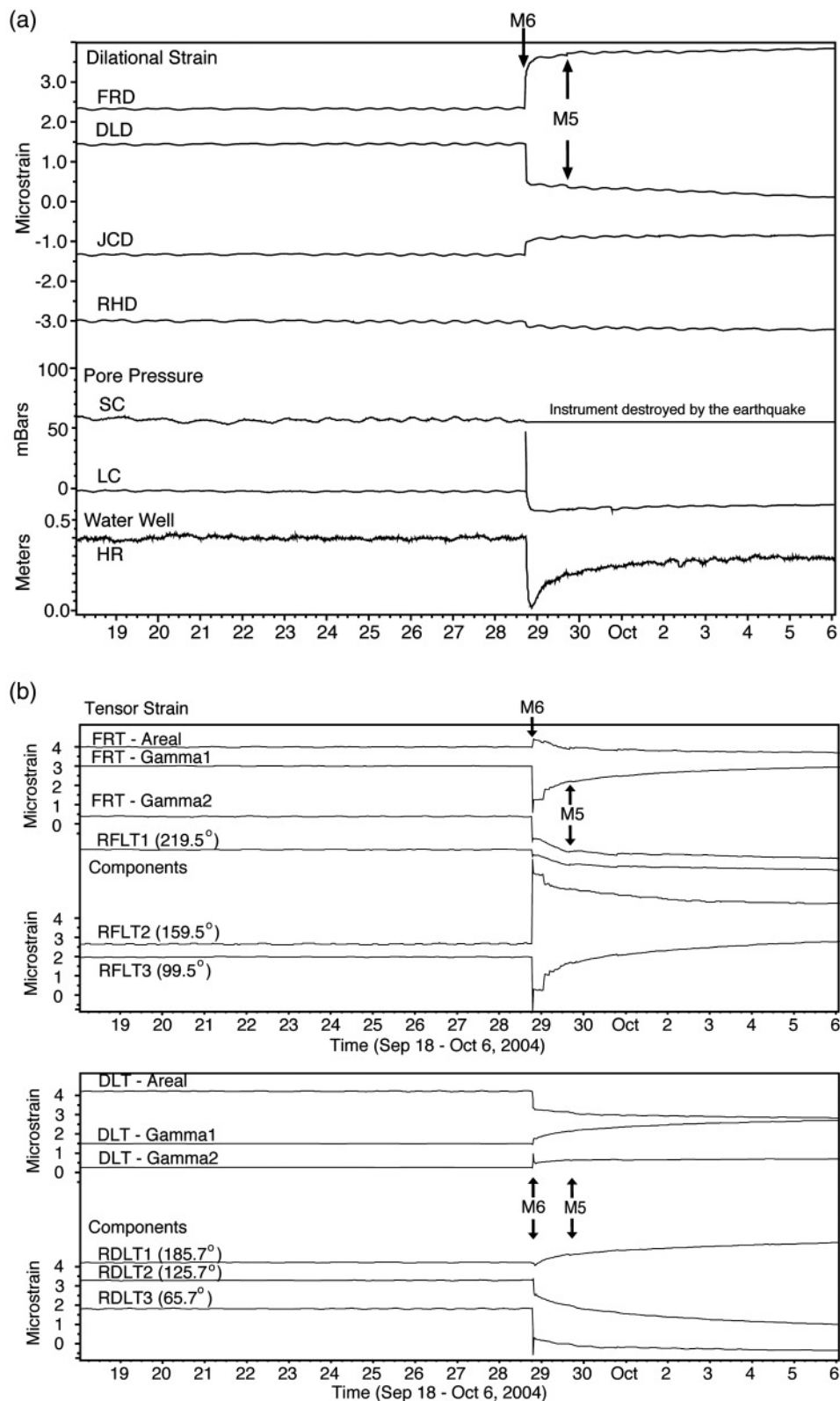


Figure 3. (a) Strain, pore pressure, and water-level data recorded at four dilational strainmeters, two pore pressure sites, and one operating water well near the peak rupture from 18 September 2004 to 6 October 2004 before and after the *M* 6.0 28 September Parkfield earthquake. Contraction is positive. Strain offsets on opposite sides of the fault produced by the earthquake have opposite signs. These 10-min sampled data have atmospheric pressure loading and instrument resets removed. (b) Areal and shear strain data together with original component data recorded at the two tensor strainmeters from 18 September 2004 to 6 October 2004, before and after the *M* 6.0 28 September Parkfield earthquake. Note that contraction is positive. These data have instrument resets removed. All data are displayed with identical vertical scales in microstrain. Sample rates are every 10 min for the dilatometers, every 18 min for DLT, and every 30 min for FLT. Numbers following the component label refer to the orientation clockwise from north for that component.

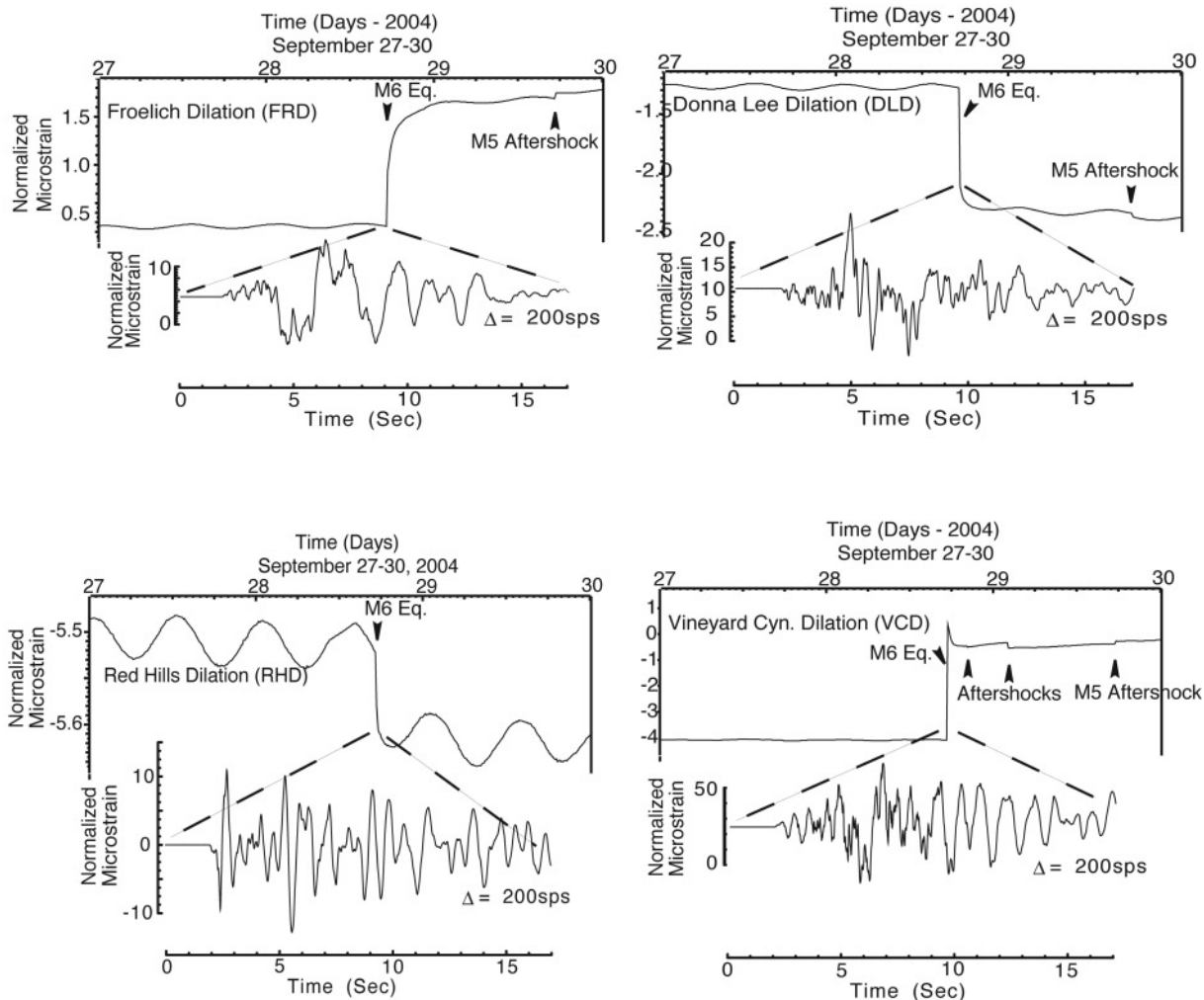


Figure 4. One and a half days of data from four dilational strainmeters before and after the earthquake together with strain and acceleration data samples at 200 sps showing the strain seismogram. Note that the strainmeter scale factors are derived from earth tide calibration and are termed normalized. In contrast, strain scale factors used by Borchardt *et al.* (2006) are the mechanical scale factors of the strainmeters.

Table 2
Observed Coseismic Dilational Strain Offsets* for the 2004 Parkfield Earthquake

Site	Latitude	Longitude	Dilation	Areal Strain
Dilational Strainmeters				
FRD	35.9108	-120.4883	+0.61	+0.41
DLD	35.9401	-120.4234	-0.84	-0.56
JCD	35.7153	-120.2064	+0.284	+0.189
RHD	35.6244	-120.2577	-0.058	-0.038
VCD	35.9219	-120.5355	+4.776	+3.184

*Compression positive in microstrain.

Table 3
Observed Coseismic Tensor Strain Offsets* for the 2004 Parkfield Earthquake

Site	Latitude	Longitude	Areal		
			Strain	Gamma 1	Gamma 2
Tensor Strainmeters					
FRT	35.9107	-120.4859	+0.425	-2.33	-1.5
DLT	35.9401	-120.4234	-0.85	+0.51	+0.71

*Compression positive in microstrain.

Table 4
Model Parameter for Uniform Slip Model Obtained from Inversion of Strain and GPS Displacement Data

Fault	Latitude	Longitude	Strike	Dip	L	W	Slip
					(km)	(km)	(m)
San Andreas Fault	38.836	-120.372	143°	90°	15	6	0.35

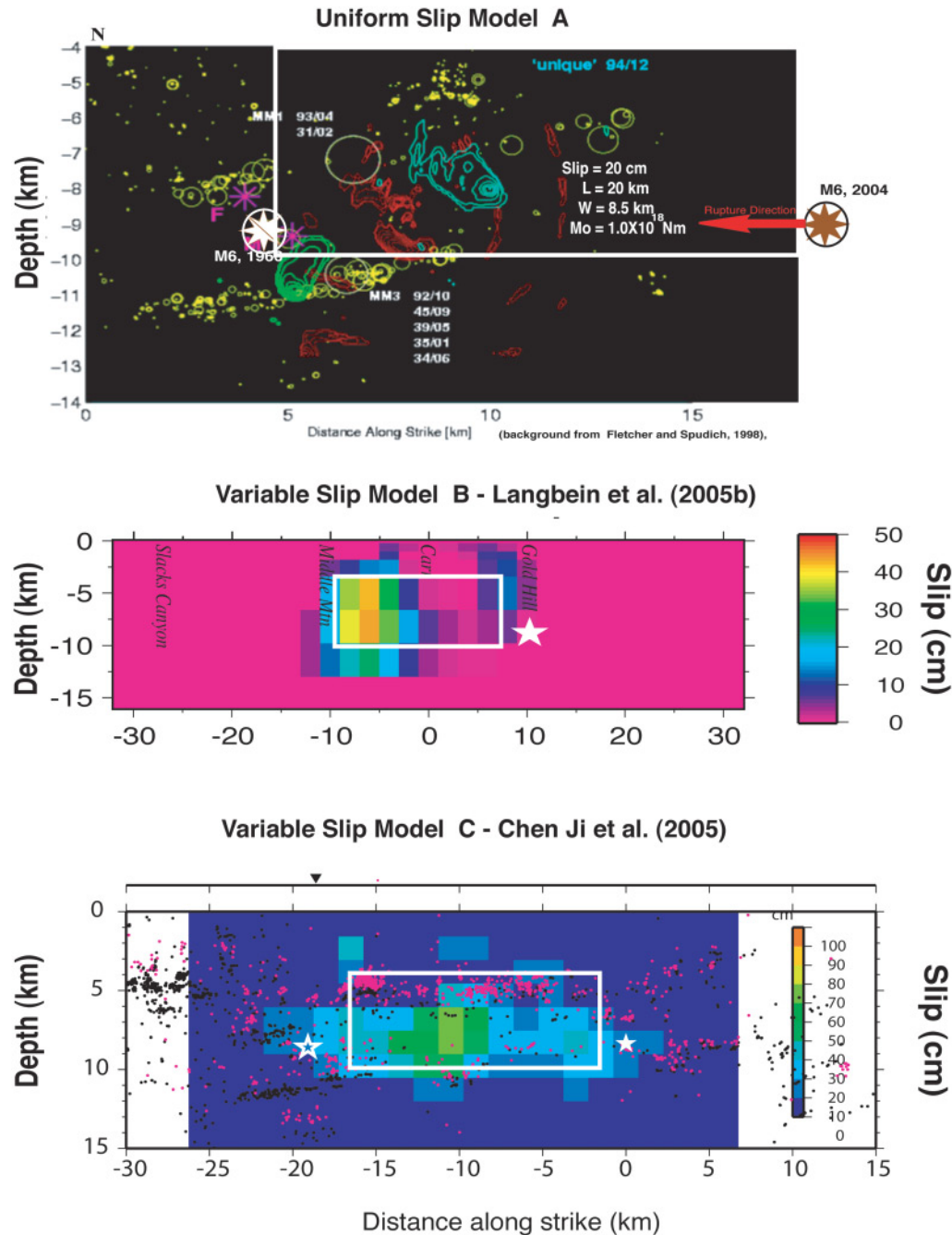


Figure 5. Uniform slip model obtained by inversion of strain and GPS data for the Parkfield earthquake and variable slip models from Langbein *et al.* (2006) and Chen (2004) obtained by inversion of GPS data for the Parkfield earthquake. To allow comparison, the outline of the uniform slip model is superimposed on each of the variable slip models.

aliased into the coseismic offset data (Langbein *et al.*, 2006). An interesting issue exists with the strong-motion model of Lui *et al.* (2006), for which substantial shallow slip occurs to the north of DLD and FRD sites near the SC and LC pore pressure sites (Fig. 1). In this region, the GPS model of Langbein has been constrained to have zero slip because of poor

coverage. However, this slip patch could explain the large 4.8 microstrain contraction at VCD, which is poorly fit in the current GPS-based models. Comparative discussion of the different models can be found in Liu *et al.* (2006). Clearly, further integration and consolidation of all these different models and data is needed.

Preseismic Strain, Displacement, and Pore Pressure

The issue of precursory activity is a crucial one. Laboratory observations and modeling efforts suggest that fault failure occurs when displacements exceed those for peak shear stress. Accelerating strain resulting from increased deformational weakening occurs before the dynamic slip instability that results in an earthquake. In rock mechanics terminology, this stage is called tertiary creep (Jaeger and Cook, 1976; Lockner, 1998). In terms of laboratory determined rate or state dependent friction (Dieterich, 1994; Ruina, 1983), it is called slip weakening. That nonlinear strain precedes rupture has provided hope that detection of these strain changes will lead to a method for earthquake prediction. The form of strain change expected is exponential-like with the largest strain changes occurring at the last stages of failure and the amplitude or size of the strain change relates to nucleation patch moment release. If the nucleation moment release is detectable, these observations could be used as a technique for earthquake prediction. Unfortunately, continuous strain measurements near moderate to large earthquakes thus far have failed to detect any indications of exponentially increasing strain (Abercrombie *et al.*, 1995; Johnston *et al.*, 1990, 1994; Wyatt *et al.*, 1994). This implies the scale must be small compared to the eventual rupture size. The Parkfield **M** 6.0 earthquake is the best instrumented earthquake so far on which to test these conclusions.

To search for very small changes in strain immediately before the earthquake, earth tides with ocean-loading components (Agnew, 1997; Tamura, 1991) and atmospheric pressure loading (Rabbel and Zschau, 1985) must first be predicted and removed from the data using least-squares methods. Great care must be taken to avoid having the coseismic offsets contaminate the least-squares fitting. The primary technique used here was to remove the coseismic offsets and immediate postseismic changes, replace these data with predicted tidal data, then fit and remove the tides. Only corrected data up to the time of the earthquake was then considered. Other tide removal techniques were also tried but no improvement in noise reduction was achieved.

Figure 6 shows strain, pore pressure, and water-well data after atmospheric pressure loading and earth tides have been predicted and removed from the data. The strain units are nanostrain, the pore pressure units are millibars, and the water-well data are in meters. Note that data for tensor instrument FRT are not included here because the residual noise level after removal of tides and atmospheric pressure exceeds 10 nanostrain. There are some hints of changes in the last day preceding the earthquake, and an immediate worry was that these resulted in some way from the processing. This was probably not the case since firstly, different processing gave similar results, and secondly, all instruments recorded offsets that were subjected to the same processing but not all show slow changes. A further complication arises since the largest change of 8 nanostrain oc-

curred on the FR dilatometer and this instrument reset itself also about 24 hr before the earthquake (Fig. 6). This reset introduced a small amount of heating as shown during other resets on this instrument. If these FR data are removed, the next largest change is in pore pressure at SC. Curiously, this measurement site is well outside the rupture area. While this change is significant in this section of record, such changes have occurred at other times. Overall, none of these changes are significant in the longer term record and the form of the changes are not what would be expected on the basis of theory and laboratory observations for nucleation at the earthquake hypocenter. Nevertheless, the possibility that they may result from another process such as deeper larger-scale slip episode on the San Andreas that triggered the earthquake cannot be precluded.

An additional indicator whether preseismic strain changes occurred comes from the shorter-term data immediately before the earthquake. These data were recorded in the preevent memory of the high sample rate triggered recorder (Borchardt *et al.*, 2006) and are shown in Figure 7a for the 20 sec (left) and 1 sec (right) before the earthquake after low-pass filtering the data with a 5-pole butterworth filter with a high cut of 10 Hz. The units are nanostrain for the 20-sec plot and picostrain for the 1-sec plot. While coherent changes of 20 picostrain would be readily apparent in these data, there are no indications of short-term accelerating strain on either plot near the time of the actual earthquake occurrence. In contrast, the strain change during the earthquake was more than 1 microstrain or more than five orders of magnitude larger. If nucleation slip/moment release occurred at the earthquake hypocenter, then it must be correspondingly five orders of magnitude smaller than the coseismic moment. Figure 8 shows nucleation moment release from a point source as a function of depth within the earthquake rupture zone for strainmeter measurement resolution at different periods where the strainmeters are located at depth/2 from the fault. The Parkfield earthquake (star) occurred at a depth of 8 km. At periods of seconds, the resolution was about 0.01 nanostrain, and the largest moment release that could go undetected would be $2 > 10^{12}$ N m. This would be equivalent to about a **M** 2.0 earthquake.

Even better data might have been obtained if the two instruments at Gold Hill (GH) had remained operational. These instruments at different distances from the fault were near the eventual earthquake epicenter. However, while the strainmeters at GH failed, the high-quality acceleration and velocity data at this site continued to be collected. Ground displacements preceding the earthquake were determined from the acceleration data at GH and other sites (Borchardt *et al.*, 2006), and these data provide independent constraints on nucleation size. Displacement data at just the strainmeters sites are shown in Figure 7b together with their standard deviations during the 20 sec and 2 sec before the *P*-wave arrivals. Clearly the most important is these sites is GH at the earthquake epicenter. The standard deviation in displacement here was 0.5×10^{-8} m. In contrast, the coseismic

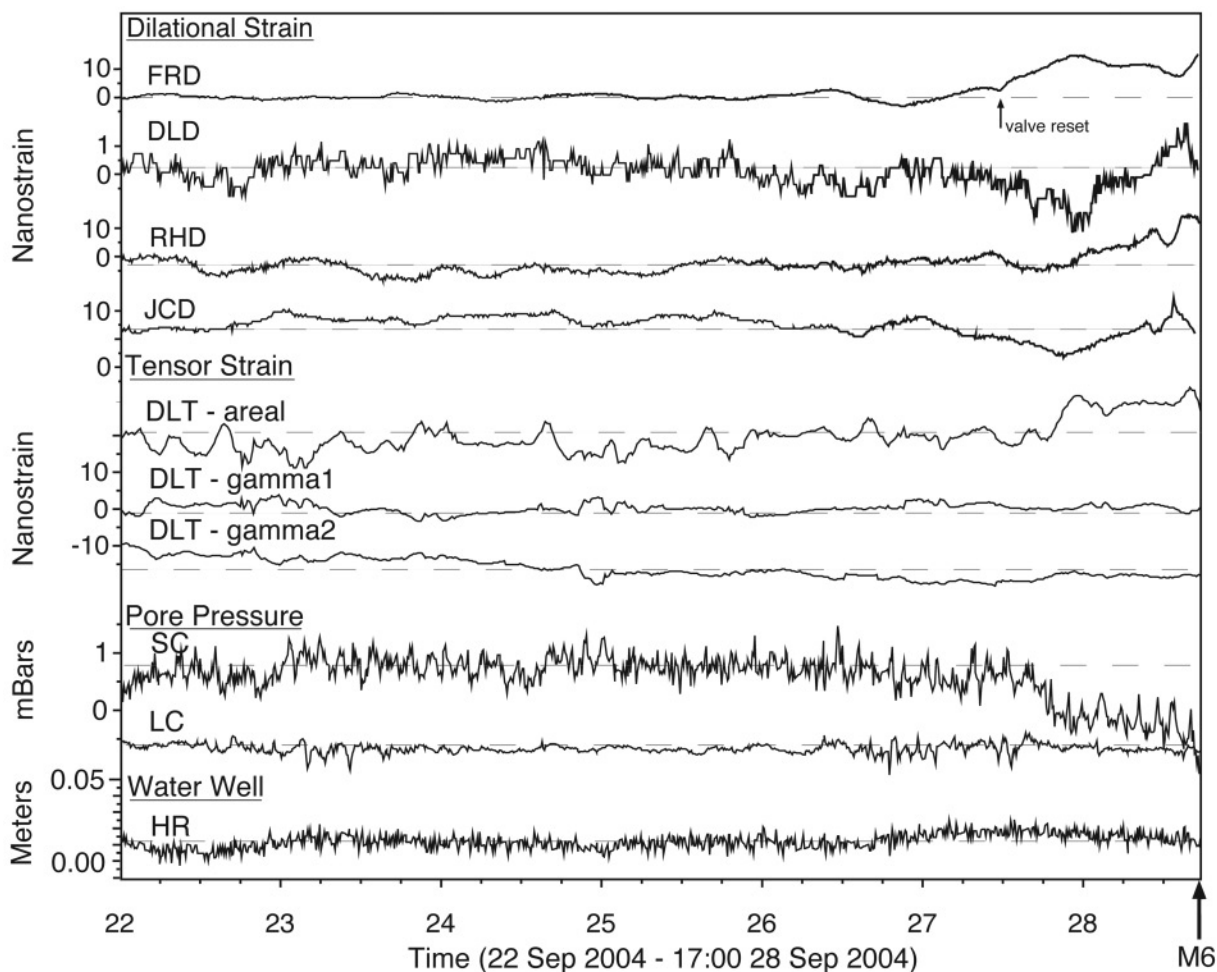


Figure 6. Dilational strain, tensor strain, pore pressure, and water level during the week before the M 6.0 Parkfield earthquake. Atmospheric pressure loading and instrument resets have been removed from these data. Note that data for tensor instrument FRT are not included here because the residual noise level after removal of tides and atmospheric pressure exceeds 10 nanostrain. Arrow shows the occurrence time of the earthquake.

displacement estimated from the GPS data at this site is 0.05 m. This is six orders of magnitude larger than displacements observed immediately before the earthquake. Similar ratios are obtained at other strainmeter sites and other sites throughout the region. This consistent with conclusions based on the strainmeter data and implies a nucleation moment release during this time that is even smaller than estimates from the strain data.

Postseismic Strain

Significant postseismic compressive strain appears to have occurred during the 12 hr following the earthquake (see Fig. 3a, b), and this has continued in the months following the earthquake. The erratic postseismic response of the FRT instrument may indicate that this instrument is failing. During this postseismic period, slip varies as log (time) consis-

tent with continued slip on the earthquake rupture plane in response to incomplete reduction of plate loading stress and expanding slip into the near-surface region after stress-induced velocity strengthening (Scholz, 1990). Langbein *et al.* (2006) fit time constants from these data to an Omori decay law expected from a velocity strengthening friction law expected from faults with stable creep (Perfettini and Avouac, 2004), as occurs in this Parkfield region.

Tidal Response

Ocean-load-corrected earth tides are used to calibrate both the strain instruments and the region near the instruments. Since the mechanical calibration of the instruments is known, comparison of ratios of tidal to mechanical calibration at different sites gives a measure of differences in bulk modulus between instruments in the fault zone with

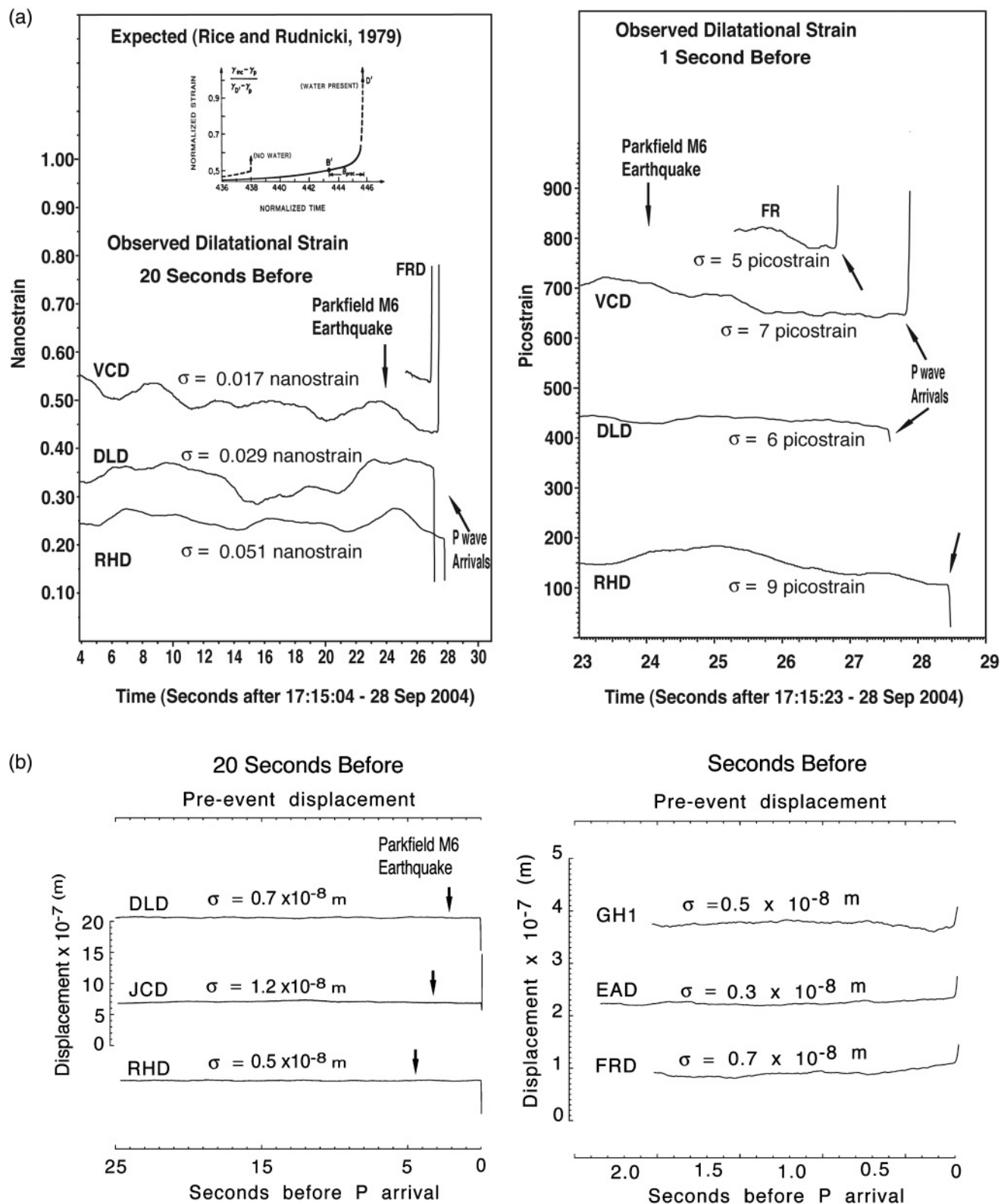


Figure 7. (a) Expected strain time history before rupture from Rice and Rudnicki (1979) together with observed dilational strain during the 23-sec and 1-sec periods before the M 6.0 Parkfield earthquake. Standard deviations σ up to the time of the first P arrival are included on each plot. Strain changes immediately before the earthquake are less than 10 picostrain. Arrows show the occurrence times of earthquakes. (b) Ground displacement derived from acceleration data (from Borchardt *et al.*, 2006) during the period 20-sec and 1-sec before the M 6.0 Parkfield earthquake. Each trace has the peak change in displacement during these periods listed. Strain changes immediately before the earthquake at sites close to the rupture, particularly Gold Hill (GH) near the earthquake epicenter, are less than 0.05 microns. In contrast, coseismic displacements from GPS on opposite sides of the fault from the earthquake are about 50,000 microns (Langbein *et al.*, 2005).

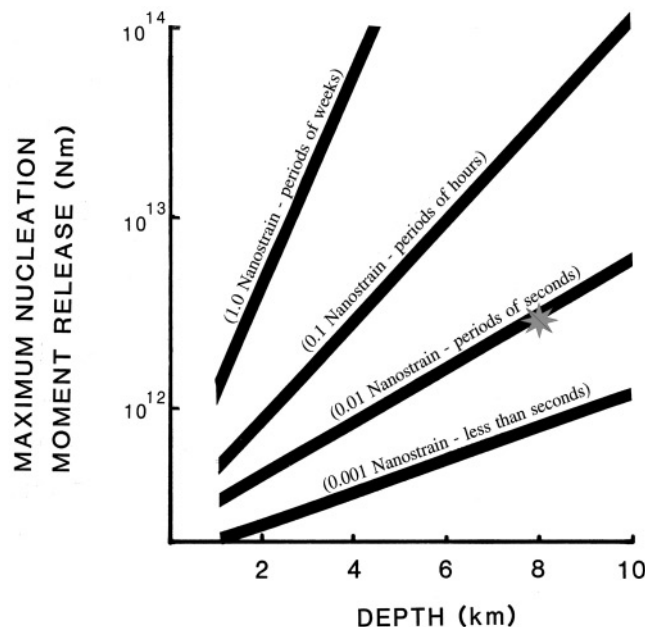


Figure 8. Maximum possible nucleation moment release from a point source slip model (Okada, 1992) as a function of nucleation source depth for different strainmeter resolutions in nanostrain at different periods. At periods of seconds, the resolution is 0.01 nanostrain, at periods of hours it is 0.1 nanostrain, and at periods of weeks, it is 1 nanostrain.

others in crustal materials at tens of kilometers from the fault. Examination of comparative ratios of tidal amplitudes of the San Andreas Fault indicates differences in the ratios of not more than a factor of two, as suggested by Johnston *et al.* (1994) from tidal response near the 1992 M 7.3 Landers earthquake and Fialko *et al.* (2002) from INSAR data near the 1999 M 7.1 Hector Mine earthquake. In other words, if the material in the San Andreas Fault is more compliant than the surrounding region, it does not differ by more than about a factor of two or three. The strain-offset data that are based on these calibrations do not reflect obvious strain amplification. The data could be consistent with a modulus contrast of a factor of two or three, and this may still be sufficient to produce the blocklike behavior necessary to explain the geologic, geodetic, and data on trapped seismic waves in the fault zone (Yong-Gang *et al.*, 2002).

A further question remains whether material properties might have changed prior to the earthquake, as indicated by changes in earth tidal response. This technique was first suggested by Nishimura (1950) as a possible means for earthquake prediction. Following techniques discussed in Linde *et al.* (1992), we have determined the tidal response for the two years prior to the earthquake and find no significant change in this response with time for this earthquake. A plot of M 2.0 amplitude as a function of time from 2003 to the present is shown in Figure 9. Higher noise at certain times reflects bad data. No change in tidal response is apparent in the data before the earthquake. Changes following the earth-

quake probably reflect the effects of coseismic and postseismic slip. This result is consistent with similar observations during the Loma Prieta earthquake (Linde *et al.*, 1992).

Tremor

Unusual nonvolcanic tremor events have been observed on a high-resolution seismic network installed to monitor the Parkfield region (Nadeau and Dolenc, 2004). These events had been previously observed on subduction zones (Rogers and Dragert, 2003) and suggested to be related to slow slip or slow earthquake events. Fortunately the Parkfield tremor events are located immediately beneath two of the borehole strainmeters sites as shown in Figure 10. The strainmeters are ideally suited for detection of slow earthquakes. A number of these slow events at a depth of 4–8 km have been observed with associated aftershocks further north on the San Andreas Fault (Linde *et al.*, 1996; Johnston and Linde, 2002). Records from the two strainmeters have been searched during the total 175 reported tremor events from January 2001 to March 2005 (R. M. Nadeau, personal comm., 2005).

The strain data for two of the largest events are shown in Figure 11 (upper), while the composite plot showing strain for all events is shown in the lower plot. It is apparent that there are no strain changes at the time of these events although there are some hints that these events occur at peak tidal extension. Because of the depth of the tremor events between 20 and 40 km, these data do not place a tight constraint on aseismic moment release that might accompany the events. It is possible that slip equivalent to a M 3 earthquake could accompany the tremor events and not be detected on the strainmeters. Clearly this situation is very different from the equivalent M 5 aseismic, or slow earthquake, events that occurred on the San Andreas Fault near San Juan Bautista (Linde *et al.*, 1996) with accompanying microseismicity whose total moment release was one to two orders of magnitude less.

Discussion

It is clear that for the 2004 Parkfield earthquake, no significant precursory strain, pore pressure, or displacement changes preceded this event, either in the intermediate term or in the short-term (sec) when the expected signal should be largest. Similar results have been obtained in the near field (i.e., less than one rupture length) of other moderate to large earthquakes in California (Agnew and Wyatt, 1989; Johnston and Linde, 2002; Johnston *et al.*, 1987, 1990, 1994; Linde and Johnston, 1989; Wyatt *et al.* 1994). There are some hints of changes in strain and pore pressure rate in the 24 hr before the event. The largest of these is questionable because of an instrument reset, and all of the others are not significant when compared with longer-term data. These signals are intriguing since they could result from other broader

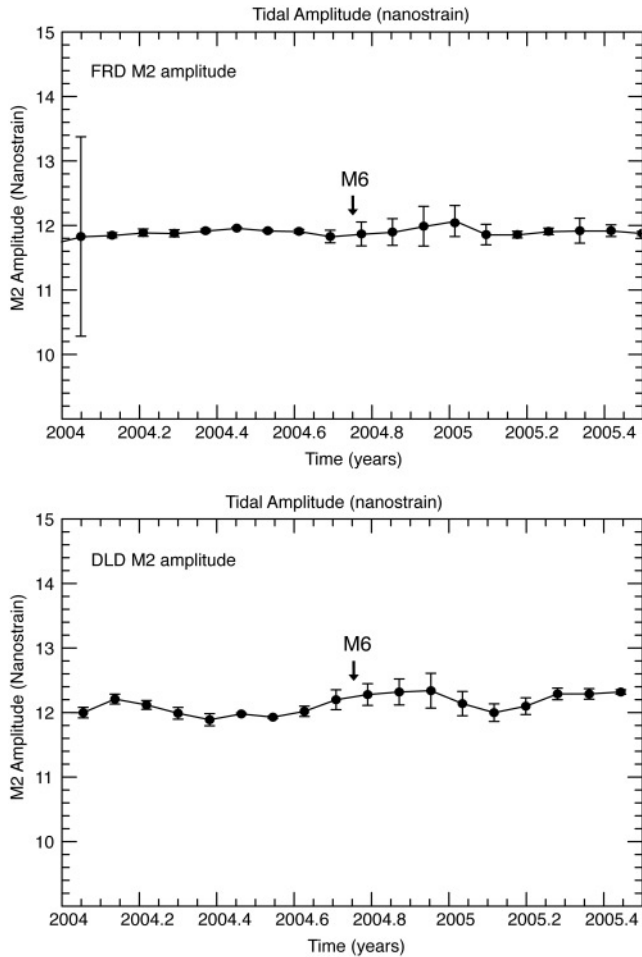


Figure 9. M2 tidal response as a function of time at the two sites FRD and DLD on either side of the rupture. Sliding 2-month time blocks were used with a 50% overlap between blocks. Error bars are 1 standard deviation.

scale (deeper) activity on the fault that may have triggered the earthquake, but we are unable to constrain the details.

During the last seconds before the Parkfield earthquake, the maximum moment release on faults that subsequently ruptured could not have been more than 2×10^{12} N m. This is less than 0.001% of the moment release during the earthquake since moment release at the earthquake hypocenter during this time was 10^{18} N m. Preevent displacements obtained from accelerometers at Gold Hill immediately above the hypocenter indicate the nucleation moment release were even smaller at 10^{-7} , or less than 0.0001%, of the earthquake moment.

How big might the nucleation zone be? If we assume displacement, U , is proportional to rupture length, L , as indicated by both observation and theory (constant stress drop assumption) for earthquakes with M_L less than 6 (e.g., see Scholz, 1997). Then,

$$U = KL \Delta\sigma, \quad (1)$$

where $K \approx 10^{-7}$ m/MPa/km, L = rupture dimension, and $\Delta\sigma$ = stress drop (approx 3 MPa). Therefore, the moment M is given by:

$$M = \mu 10^{-4} L^3, \quad (2)$$

where μ is the rigidity. For a nucleation size of 2×10^{12} N m obtained from the strain data, the nucleation source size would be <100 m. For a moment 10 times smaller indicated by the GH displacement data the size would be 46 m. Alternatively, using the empirical relations from Aki (1987),

$$\text{Log}(M_0) = 2M_L + 14.2 - \text{Log } \Delta\sigma \quad (3)$$

$$\text{Log}(L) = 0.6M_L - 2.9 - 0.6\text{Log } \Delta\sigma. \quad (4)$$

Assuming a stress drop of 3 MPa, this gives a source size of <34 m using the strain and <12 m using the displacement data. These sizes are similar to patches of repeating earthquakes observed in this region by Nadeau and McEvilly (1997) but much larger than nucleation source sizes observed in the laboratory where frictional slip on preexisting slip surfaces in large-scale laboratory friction experiments (Dieterich, 1981) indicates nucleation slip does initiate within a small nucleation region. On the other hand, Dieterich (1992) shows numerical calculations that indicate the size of these regions should be 1–10 m for both smooth or rough initial stress distributions—consistent with the upper bounds allowed by the strain and displacement data. It would appear from both data that the scale on which rupture initiates is several orders of magnitude smaller than that of the subsequent earthquake. If so, the fault model relevant to this process must be inhomogeneous in character to accommodate these observations that crustal failure does not occur simultaneously through the entire rupture zone but is apparently triggered by failure of small localized zones, indicating nucleation runaway or “cascade” runaway. This result, and similar results for other large magnitude earthquakes (Johnston and Linde, 2002), is in clear conflict with suggestions by Ellsworth and Beroza (1995) and Iio (1995) that nucleation scales with earthquake magnitude. Similar conclusions that rupture size is determined by the pattern of stress heterogeneity on the fault, not the nucleation source, were reached by Lavalée and Archuleta (2003) for the 1979 Imperial Valley earthquake. If correct, the possibility that reliable predictions can be made of the location, time, and magnitude of moderate to large earthquakes does not seem likely.

The strain and pore pressure data similarly constrain changes in pore pressure in the fault zone that may be related to the failure process. If we assume no hydraulic connectivity between regions of high pore pressure on the fault zone (such as proposed by Byerlee, [1990] and Byerlee [1993]) and ignore for the moment how pore pressure changes in these regions might occur, it is obvious from simple calcu-

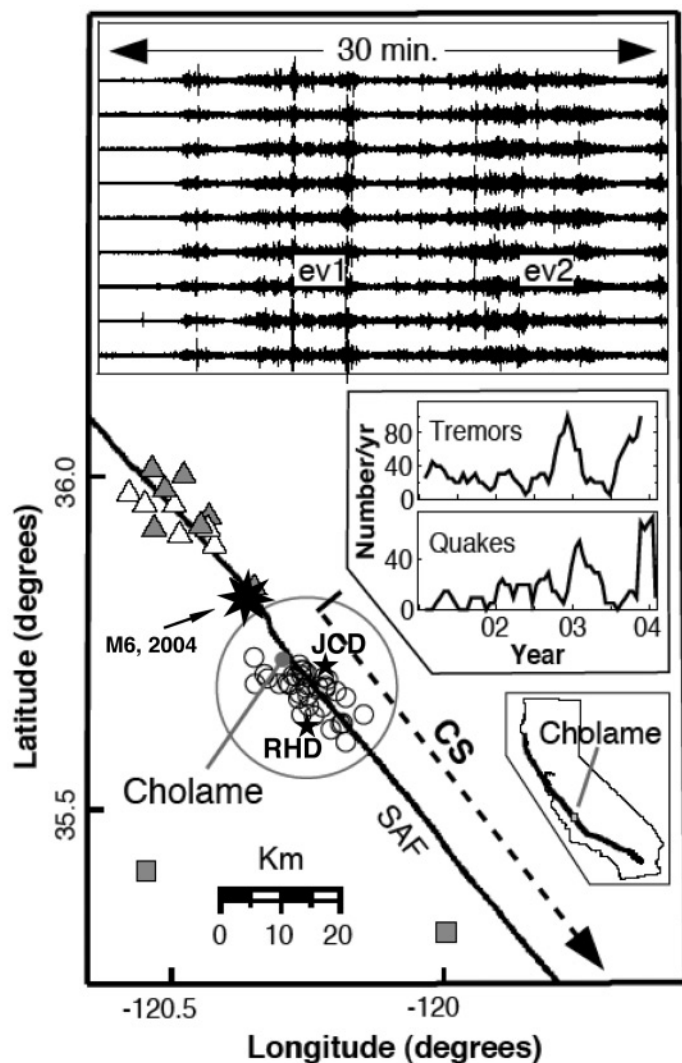


Figure 10. Locations of tremor events (circles) from Nadeau and Dolenc (2004) in relation to the 2004 M 6.0 Parkfield earthquake, nearby strainmeters JCD and RHD in the Cholame section (CS) of the San Andreas Fault (SAF). Seismometer locations are shown as triangles. See Nadeau and Dolenc (2004) for detailed discussion of events shown.

★ Strainmeters

(After Nadeau and Dolenc, 2004)

lations of strain generated by changes in pore pressure for regions with dimensions of a few hundred meters and depths of about 5 km that rapid changes in pore pressure of 0.1 MPa should be readily detected, though not necessarily recognized as such. If hydraulic communication with the surroundings does exist, smaller pore pressure changes might be detected as poroelastic strain as fluids diffuse out to greater distances, in effect increasing the source size. Small changes in the local geometry of regions with high pore pressure probably would not be detectable.

It is also apparent in these data that large-scale changes in elastic properties within the fault zone are not occurring near these instruments. If they were, we would expect changes in tidal shear strain and volumetric strain response. Observations of earthtide response before and after the largest earthquakes (1992 M 7.3 Landers, 1989 M 7.1 Loma Prieta, etc.) indicate that if measurable changes occur, they are less than 5% (Linde *et al.*, 1992). There are no suggestions of any permanent change.

The Parkfield earthquake was modeled as slip on a uniform slip patch by inversion of GPS and strain data. The details of the slip model are listed in Figure 3. Much better distributed slip models were obtained by inversion of seismic and geodetic data (Chen *et al.*, 2004; Dreger *et al.*, 2004), geodetic (Langbein *et al.*, 2006; Murray and Langbein, 2006; Murray *et al.*, 2004) and strong-motion data (Liu and Archuleta, 2004; Liu *et al.*, 2006). The models from Langbein *et al.* (2006) and Chen *et al.* (2004) are shown in Figure 5. At this point, the best fit is to the Langbein *et al.* (2006) model. Joint inversion using all data seems necessary to improve these models together with careful correction of the GPS data for contamination from postseismic slip. It is likely that the overall model in the 20-km section north of Gold Hill will be unchanged, but small adjustments in the slip distribution near the strainmeters will result in a better fit the strain data.

The postseismic effects reflect strain redistribution in the region as fault slip continues to grow in response the

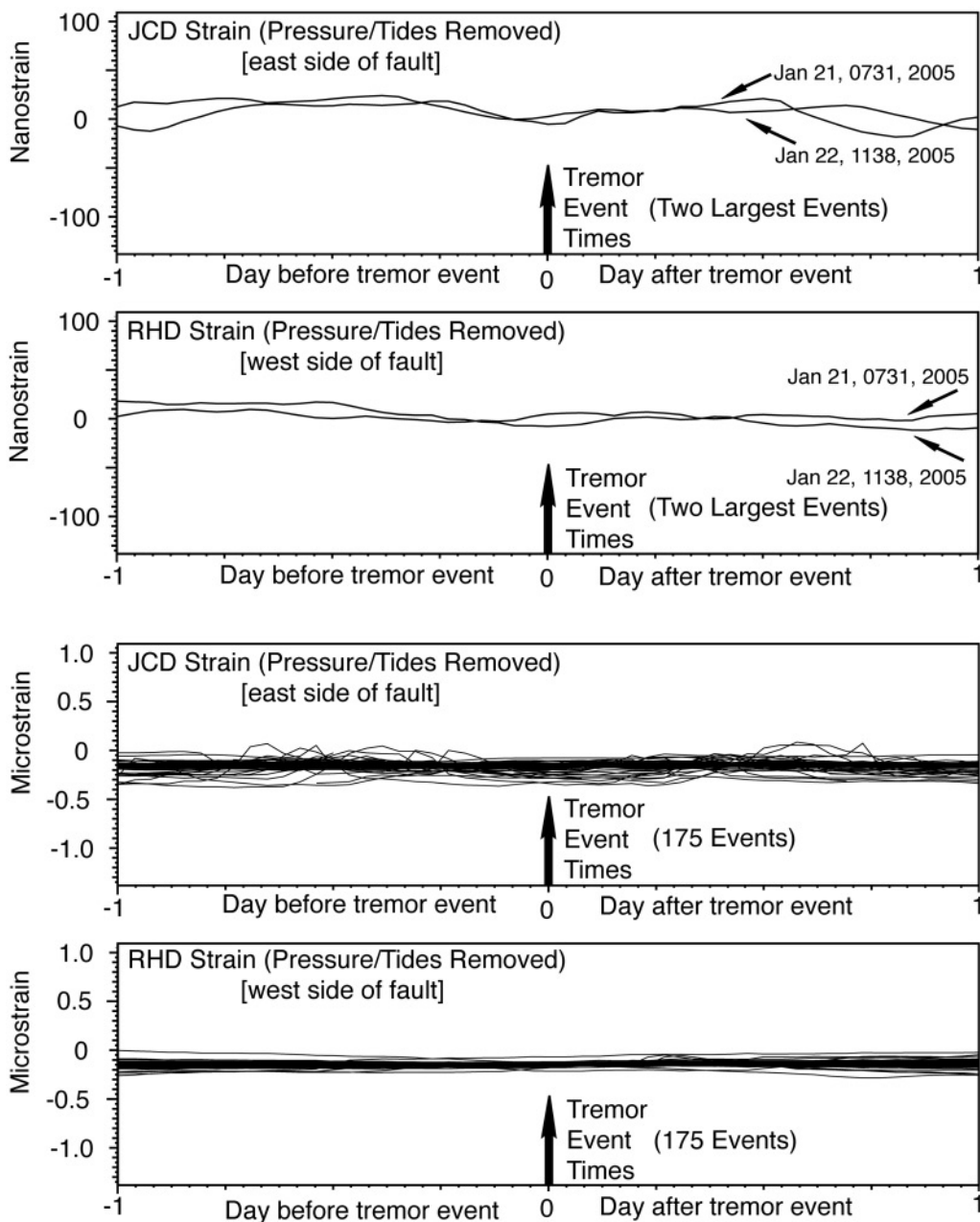


Figure 11. Strain records for the day before and after two of the largest events (left) and during 175 tremor events (right).

earthquake induced stress and incomplete release of stress from plate loading in the region. Except at DL, these strain changes are in the same sense as the coseismic offset. The relaxation time constants have been obtained by fitting an Omori Law decay to these, creep, and GPS data by Langbein *et al.* (2006).

Conclusions

The M 6.0 Parkfield earthquake occurred within a tight array of high-resolution geophysical instruments in Park-

field. These include four borehole dilational strainmeters, two borehole tensor strainmeters, two borehole pressure monitors, one water well, a network of creepmeters, and GPS displacement monitors. These data are augmented with on-site measurements of seismic acceleration and velocity (Borchardt *et al.*, 2006). The earthquake and its subsequent rupture occurred well within the array of instruments. In the hours to minutes before this event, there are no indications of significant precursive strain in these data at strain resolutions of better than 0.1 nanostrain due to precursive slip on the eventual Parkfield rupture, although some slow, mi-

nor, but not significant strain changes of perhaps a few nanostrain occurred in the 24 hr before the earthquake. In the last seconds before failure, strain resolution was 0.01 nanostrain.

The absence of measurable precursory strain changes place important constraints on possible moments and dimensions of nucleation events. The strain data could allow a nucleation moment of $2 > 10^{12}$ N m corresponding to a source size of about 34–100 m depending on the model used for this calculation, while displacement data derived from acceleration data constrain the moment to be 10 times less and source size to be 10 m or so. These moments are at least five orders of magnitude less than that of the subsequent earthquake. These upper estimates of source size are comparable to dimensions of clusters of repeating microseismicity in the region (Nadeau and McEvilly, 1997).

The apparent small size of the rupture initiation moments compared to the total earthquake moment suggests that there is no scaling of the nucleation process with earthquake magnitude. This is inconsistent with suggestions by Ellsworth and Beroza (1995) and Iio (1995) that nucleation scales with earthquake magnitude. The basic failure process thus apparently involves rupture nucleation runaway. High pore pressure fluids may be associated with this process (Byerlee, 1990, 1993) but if pore pressure changes drive the nucleation process, these changes were apparently small for the 2004 Parkfield earthquake.

The latest variable slip models of the earthquake obtained by inverting all available GPS data overestimate the coseismic strain offsets. Usually coseismic strain offsets are in relatively good agreement with geodetic models. This earthquake had a large component of postseismic slip, and it is evident that, even 5 min after the earthquake, the offsets had grown by as much as 70% of that during the earthquake. Furthermore, the strainmeters were close to the rupture and small changes in geometry and amount of slip close to the strainmeters produce large changes in strain. The possibility exists that the GPS displacements averages may be contaminated by the postseismic slip and estimates of the moment are correspondingly high.

A clear postseismic slip response has been observed, reflecting continuing slip following large earthquakes where accumulated strain energy has only been partly released. During this postseismic period, slip varies as log (time) consistent with continued slip on the earthquake rupture plane as a consequence of incomplete release of accumulated plate loading stress, expansion of slip into the near-surface region after stress-induced velocity strengthening (Scholz, 1990), and Omori Law slip decay based on a velocity strengthening friction law (Perfetti and Acouac, 2004). Afterslip is common in this region of aseismic fault slip and was observed previously following the 1966 Parkfield earthquake (Smith and Wyss, 1968).

Indications that the physical properties of the Earth's crust may have changed before, or as a result of this earthquake (Nishimura, 1950), are not supported by any observed

change in earth tide response. Tidal response is stable at the 5% level through the earthquake at the three sites with the most complete data. There are no clear indications of changes in fault zone compliance caused by the earthquake. Curious observations of nonvolcanic tremor have been reported to occur prior to and following the earthquake (Nadeau and Dolenc, 2004). The hypocenters of these tremor events were located immediately beneath two of the strainmeters in the south of the network. No measurable deformational strain (slip moment release) preceded or occurred at the time of these tremor events in contrast to the measurable strain and associated seismicity occurring with aseismic slip events, or slow earthquakes, observed elsewhere on the San Andreas Fault.

Acknowledgments

We thank Jim Savage, Mike Lisowski, John Langbein, Ruth Harris, and an anonymous reviewer for useful manuscript reviews. John Langbein and Chen Ji provided details of their variable slip models obtained from inversion of GPS data. We thank John Langbein for useful discussion, particularly about the FR valve reset; Doug Myren and Rich Leighti for critical installation and maintenance support; Marie Mee for data analysis; and Andy Snyder for resuscitating the Halliburton water well in May 2004, just four months before the earthquake.

References

- Abercrombie, R. E., D. C. Agnew, and F. K. Wyatt (1995). Testing a model of earthquake nucleation, *Bull. Seism. Soc. Am.* **85**, 1873–1879.
- Agnew, D. C. (1997). NLOADF: a program for computing ocean-tide loading, *J. Geophys. Res.* **102**, 5109–5110.
- Agnew, D. C., and F. K. Wyatt (1989). The Superstition Hills earthquake sequence: tilts and strains at Pinon Flat Observatory, *Bull. Seism. Soc. Am.* **79**, 480–493.
- Aki, K. (1987). Frequency-magnitude relation for small earthquakes: a clue to the origin of f_{MAX} of large earthquakes, *J. Geophys. Res.* **92**, 1349–1362.
- Bakun, W. H., B. Aagaard, B. Dost, W. L. Ellsworth, J. L. Hardebeck, R. A. Harris, M. J. S. Johnston, J. Langbein, J. J. Lienkaemper, A. J. Michael, J. R. Murray, R. M. Nadeau, P. A. Reasenber, E. A. Roeloffs, A. Shakal, R. W. Simpson, and F. Waldhauser (2005). Implications for prediction and hazard assessment from the 2004 Parkfield Earthquake, *Nature* **437**, 969–974.
- Borcherdt, R. D., J. B. Fletcher, E. G. Jensen, G. L. Maxwell, J. R. VanSchaack, R. E. Warrick, E. Cranswick, M. J. S. Johnston, and R. McClearn (1985). A general earth observation system (GEOS), *Bull. Seism. Soc. Am.* **75**, 1783–1826.
- Borcherdt, R. D., M. J. S. Johnston, and G. Glassmoyer (1989). On the use of volumetric strainmeters to infer additional characteristics of short-period seismic radiation, *Bull. Seism. Soc. Am.* **79**, 1006–1038.
- Borcherdt, R. D., M. J. S. Johnston, and G. Glassmoyer (2006). Recordings of the Parkfield 2004 earthquake on the GEOS strong-motion array: implications for earthquake precursors, fault rupture, coseismic, and postseismic strain changes, and characteristics of short-period seismic radiation, *Bull. Seism. Soc. Am.* **96**, no. 4b, ●●●–●●●.
- Byerlee, J. (1990). Friction, overpressure and fault normal compression, *Geophys. Res. Lett.* **17**, 2109–2112.
- Byerlee, J. (1993). Model for episodic flow of high pressure water in fault zones before earthquakes, *Geology* **21**, 303–306.
- Chen, J., K. K. Choi, N. King, K. M. Larsen, and K. W. Hudnut (2004). Co-seismic slip history and early afterslip of the 2004 Parkfield earth-

- quake, *EOS Trans. AGU* **85**, no. 47, Fall Meeting Suppl., S53D-04 (abstract).
- Dieterich, J. H. (1981). Constitutive properties of faults with simulated gouge (J. Handin Festschrift), American Geophysical Monograph, 103–120.
- Dieterich, J. H. (1992). Earthquake nucleation on faults with rate- and state-dependent friction, *Tectonophysics* **211**, 115–134.
- Dieterich, J. H. (1994). A constitutive law for rate of earthquake production and its application to earthquake clustering, *J. Geophys. Res.* **99**, 2601–2618.
- Dreger, D., M. H. Murray, and D. Oglesby (2004). Kinematic modeling of the 2004 Parkfield Earthquake, *EOS Trans. AGU* **85**, no. 47, Fall Meeting Suppl., S51C-0170I (abstract).
- Ellsworth, W. L., and G. C. Beroza (1995). Seismic evidence for a seismic nucleation phase, *Science* **268**, 851–855.
- Fialko, Y., D. Sandwell, D. Agnew, M. Simons, P. Shearer, and B. Minster (2002). Deformation on nearby faults induced by the 1999 Hector Mine Earthquake, *Science* **297**, 1858–1862.
- Fletcher, J. B., and P. Spudich (1998). Rupture characteristics of the three $M \sim 4.7$ (1992–1994) Parkfield earthquakes, *J. Geophys. Res.* **103**, 835–854.
- Gladwin, M. T. (1984). High precision multi-component borehole deformation monitoring, *Rev. Sci. Instrument.* **55**, 2011–2016.
- Hart, R. H. G., M. T. Gladwin, R. L. Gwyther, D. C. Agnew, and F. K. Wyatt (1996). Tidal calibration of borehole strain meters: removing the effects of small-scale inhomogeneity. *J. Geophys. Res.* **101**, 25,553–25,571.
- Iio, Y. (1995). Observation of the slow initial phase of microearthquakes: implications for earthquake nucleation and propagation, *J. Geophys. Res.* **100**, 15,333–15,349.
- Jaeger, J. C., and N. G. W. Cook (1976). *Fundamentals of Rock Mechanics*, Wiley, New York, 585 pp.
- Johnston, M. J. S., and A. T. Linde (2002). Implications of crustal strain during conventional, slow and silent earthquakes, in *International Handbook of Earthquake and Engineering Seismology*, Vol. 81A, Academic Press, New York, 589–605.
- Johnston, M. J. S., A. T. Linde, and D. C. Agnew (1994). Continuous borehole strain in the San Andreas Fault zone before, during, and after the 28 June 1992, M_w 7.3 Landers, California, Earthquake, *Bull. Seism. Soc. Am.* **84**, 799–805.
- Johnston, M. J. S., A. T. Linde, M. T. Gladwin, and R. D. Borchardt (1987). Fault failure with moderate earthquakes, *Tectonophysics* **144**, 189–206.
- Johnston, M. J. S., A. L. Linde, and M. T. Gladwin (1990). Near-field high resolution strain measurements prior to the October 18, 1989, Loma Prieta M_s 7.1 earthquake, *Geophys. Res. Lett.* **17**, 1777–1780.
- Langbein, J., R. Borchardt, D. Dreger, J. Fletcher, J. L. Hardebeck, M. Hellweg, Chen Ji, M. Johnston, J. R. Murray, R. Nadeau, M. Rymer, and J. Treiman (2005). Preliminary Report on the 28 September 2004, M 6.0 Parkfield, California Earthquake, *Seism. Res. Lett.* **76**, 10–26.
- Langbein, J., R. Gwyther, R. Hart, and M. T. Gladwin (1999). Slip rate increase at Parkfield in 1993 detected by high-precision EDM and borehole tensor strainmeters, *Seism. Res. Lett.* **31**, 2529–2532.
- Langbein, J., J. R. Murray, and H. A. Snyder (2006). Coseismic and initial postseismic deformation from the 2004 Parkfield, California earthquake, observed by Global Positioning System, creepmeters, and borehole strainmeters, *Bull. Seis. Soc. Am.* **96**, no. 4b, ●●●–●●●.
- Lavallee, D., and R. J. Archuleta (2003). Stochastic modeling of slip spatial complexities for the 1979 Imperial Valley, California, earthquake, *Geophys. Res. Lett.* **30**, 1245, doi 10.1029/2002GL015839.
- Linde, A. T., and M. J. S. Johnston (1989). Source parameters of the October 1, 1987 Whittier Narrows earthquake from crustal deformation data, *J. Geophys. Res.* **94**, no. B7, 9633–9643.
- Linde, A. T., M. T. Gladwin, and M. J. S. Johnston (1992). The Loma Prieta earthquake, 1989 and earth strain tidal amplitudes: an unsuccessful search for associated changes, *Geophys. Res. Lett.* **19**, 317–320.
- Linde, A. T., M. T. Gladwin, M. J. S. Johnston, R. L. Gwyther, and R. Bilham (1996). A slow earthquake near San Juan Bautista, California, in December 1992, *Nature* **383**, 65–68.
- Liu, P., and R. Archuleta (2004). A finite fault model for the 1994 M_w 6 Parkfield, California, earthquake, *EOS Trans. AGU* **85**, no. 47, Fall Meeting Suppl., S51C-0170K (abstract).
- Liu, P., S. Custodio, and R. Archuleta (2006). Kinematic inversion of the 2004 M 6.0 Parkfield earthquake including site effects, *Bull. Seism. Soc. Am.* **96**, no. 4b, ●●●–●●●.
- Lockner, D. A. (1998). A generalized law for brittle deformation of Westerly granite, *J. Geophys. Res.* **103**, 5107–5124.
- Murray, J. R., and J. Langbein (2006). Slip on the San Andreas fault at Parkfield, California, over two earthquake cycles and implications for earthquake hazards, *Bull. Seism. Soc. Am.* **96**, no. 4b, ●●●–●●●.
- Murray, J. R., P. Segall, and J. Svarc (2004). Slip in the 2004 Parkfield M 6 earthquake: comparison with previous events and implications for earthquake recurrence models, *EOS Trans. AGU* **85**, no. 47, Fall Meeting Suppl., S54B-03 (abstract).
- Nadeau, R. M., and D. Dolenc (2004). Nonvolcanic tremors deep beneath the San Andreas Fault, *Science* **307**, 389.
- Nadeau, R. M., and T. V. McEvilly (1997). Seismological studies at Parkfield V: characteristic microearthquake sequences as fault-zone drilling targets, *Bull. Seism. Soc. Am.* **87**, 1463–1472.
- Nishimura, E. (1950). On earth tides, *Trans. Am. Geophys. Union* **31**, 357–376.
- Okada, Y. (1992). Internal deformation due to shear and tensile faults in a half-space, *Bull. Seism. Soc. Am.* **82**, 1018–1040.
- Perfetti, H., and J.-P. Avouac (2004). Post-seismic relaxation driven by brittle creep: a possible mechanism to reconcile geodetic measurements and the decay of aftershocks, application to the Chi-Chi earthquake, *J. Geophys. Res.* **109**, doi 10.1029/2003JB002917.
- Rabbell, W., and J. Zschau (1985). Static deformations and gravity changes at the earth's surface due to atmospheric loading, *J. Geophysics* **56**, 1–99.
- Rice, J. R., and J. W. Rudnicki (1979). Earthquake precursory effects due to pore fluid stabilization of a weakening fault zone, *J. Geophys. Res.* **84**, 2177–2193.
- Rogers, G., and H. Dragert (2003). Episodic tremor and slip on the Cascadia subduction zone, *Sci. Express* **10**, 1126.
- Ruina, A. (1983). Slip instability and state variable friction laws, *J. Geophys. Res.* **88**, 10,359–10,370.
- Sacks, I. S., S. Suyehiro, D. W. Evertson, and Y. Yamagishi (1971). Sacks-Evertson strainmeter, its installation in Japan and some preliminary results concerning strain steps, *Papers Meteorol. Geophys.* **22**, 195–207.
- Scholz, C. H. (1990). *Mechanics of Earthquakes and Faulting*, Cambridge University Press, New York, 439 pp.
- Scholz, C. H. (1997). Size distributions for large and small earthquakes, *Bull. Seism. Soc. Am.* **87**, 1074–1077.
- Silverman, S., C. Mortensen, and M. J. S. Johnston (1989). A satellite based digital data system for low-frequency geophysical data, *Bull. Seism. Soc. Am.* **79**, 189–198.
- Smith, S. W., and M. Wyss (1968). Displacement on the San Andreas fault initiated by the 1966 Parkfield Earthquake, *Bull. Seism. Soc. Am.* **68**, 1955–1974.
- Tamura, T., T. Soto, M. Ooe, and M. Ishiguro (1991). A procedure for tidal analysis with a Bayesian information criterion, *Geophys. J. Int.* **104**, 507–516.
- Wyatt, F. K., D. C. Agnew, and M. Gladwin (1994). Continuous measurements of crustal deformation for the 1992 Landers earthquake sequence, *Bull. Seism. Soc. Am.* **84**, 768–779.
- Yong-Gang, Li, J. E. Vidale, and E. S. Cochran (2004). Low-velocity damaged structure of the San Andreas fault at Parkfield from fault zone trapped waves, *Geophys. Res. Lett.* **31**, L12S06, doi 10.1029/2003GL019044.

Continuous Borehole Strain and Pore Pressure in the Near Field of the 28 September 2004 M 6.0 Parkfield Earthquake

17

U.S. Geological Survey ms977
345 Middlefield Road
Menlo Park, CA 94025
(M.J.S.J., R.D.B.)

Dept. Terrestrial Magnetism
Carnegie Institution of Washington
5241 Broad Branch Road NW
Washington, DC, 20015
(A.T.L.)

GTSM Technologies
Brisbane, 4069
Australia
(M.G.)

Manuscript received 20 September 2005.